Detecting Cellphone Camera Status at the Distance by Exploiting Electromagnetic Emanations

Baki Berkay Yilmaz*, Elvan Mert Ugurlu*, Milos Prvulovic† and Alenka Zajic*
*School of Electrical and Computer Engineering
Georgia Institute of Technology, Atlanta, Georgia 30332–0250
Email: byilmaz7@gatech.edu
†School of Computer Science
Georgia Institute of Technology, Atlanta, Georgia 30332–0250

***Abstract*—This paper investigates unintended radiated emissions from cellphones to identify operational status of rear/front camera. We implement a supervised learning method to achieve our goal. In the training phase, we collect data for possible combinations of phone model and camera status. Then, we apply two-phase-dimension-reduction method for better and effective classification. The first dimension-reduction phase is averaging magnitudes of frequency components of a sliding window, which is followed by applying principle component analysis (PCA) technique to reduce the dimension further. In testing phase, k-Nearest-Neighbors (k-NN) algorithm is utilized to classify test data. Finally, we provide examples to show that emanated EM signals from cellphone cameras can exfiltrate useful information.**

***Index Terms*—Side/Covert Channels, Electromagnetic Emanations, Security, Classification.**

I. Introduction

Legitimate hardware/software activities in a computer system can emit signals because of systematic changes while executing scripts, branches, codes, etc. These unintentional emissions generate a side channel that can help a sophisticated attacker exfiltrate sensitive information once detected and processed [1]. Side/covert channel attacks exploit timing differences in a program execution of different bits [3], [4], temperature variations [5], power fluctuations while signing the secret key of a cryptosystem [6]–[9], acoustic signals generated while printing a document [10], cache-misses [11], [12], etc. Although these side channels pose significant security threats, they all require direct access to the system or have relatively low bit transmission rate.

However, electromagnetic (EM) side channels circumvent these problems because 1) attacks based on emanated EM signals only require close proximity, or 2) these channels have higher bit-transmission rate compared to other physical side channels [13]. To comprehend the severity of these side channels, many attack scenarios [**?**], [14]–[16], and different leakage quantification methods [17], [18] are introduced. One interesting application of side channels is shown by Eck in 1985, where he successfully reconstructed the video content from video display unit on BBC [19]. He performed the experiments from the ground floor while the video unit was on the eighth floor. Kuhn in [20] demonstrated the severity of leakages from display units by reconstructing images on cathode-ray-tube. Although reconstructing the content of video displays is an open problem for modern devices, i.e., smartphones, these studies have created considerable interest in monitoring even more sophisticated devices by exploiting emanated signals from different units, i.e., camera. For example, identifying whether the camera of a mobile device is active or not is an interesting practical application. Many museums prohibit photography on the premises, yet through the integration of cameras on mobile devices, cameras are easily accessible and it is difficult to enforce this rule. Therefore, detecting active cameras on the premises has become an untraceable task for the museums. Similarly, detecting unauthorized recording during movie screenings is an increasingly difficult task. In addition to those, detecting hidden cameras in a given setting is another useful application of camera activity monitoring.

In this paper, we investigate the relationship between the emanated EM signal and the camera status. To achieve this goal, we first introduce the *two-phase-dimension-reduction* method to reduce the data size and prevent complex clustering operations. Then, we apply PCA to reduce the dimension of the data further, and to create a model for the proposed supervised learning method. Finally, k-NN is utilized to classify test signals. Our results demonstrate that accurate estimation for camera status is possible even from a distance of 5 meters.

The rest of the paper is organized as follows: Section II introduces the dimension reduction method and model generation. Section III implements classification method of the test signals. In Section IV, experimental results are provided for both far-field and near-field measurements, and Section V concludes the discussion.

II. Signal Acquisition and Template Generation

Earlier work shows that cellphones are complex devices with many sources of electromagnetic (EM) emanations [13]. Since our goal is to identify the status (on/off) of cell phone cameras as well as the model of the cellphone, we need a method that only keeps the emanated signals due to the camera activity while eliminating emanated signals from other parts

This work has been supported, in part, by DARPA LADS contract FA8650-16-C-7620. The views and findings in this paper are those of the authors and do not necessarily reflect the views of DARPA.

of the cell phone. Furthermore, disclosing the status of a camera and the corresponding cellphone with high accuracy requires long data instances. Therefore, number of samples taken while capturing emanated signals is generally very large and this leads to a very high dimensional input space with plethora of features. In order to address the challenges caused by the unrelated EM emanations and the large size of the input space, we propose a new method called two-phase-dimension-reduction.

A. Phase-I: Noise and Size Reduction with Windowing

Any transmitted signal is corrupted by channel noise and interference. Various signal processing techniques can be applied to minimize these impairments of received signal [22]. Also, sophisticated devices emit EM signals from almost all of its components that destruct the received signal further [23].

To reduce the effect of interference and additive noise, and hereby to increase the estimation accuracy, we first capture the signal for T seconds (the status of the phone is assumed to be kept the same during this time period). Denoting the sampling time of the measuring device as T_s, we obtain $M = T/T_s$ samples for each measurement. M is typically a large number to process. As mentioned earlier, the corresponding signal is also exposed to corruptions due the other activities and channel noise. To handle these problems, we propose to average short time discrete frequency domain transform (STFT) with a rectangular window function. Let N be the size of the window, N_S be the number of samples that do not overlap at each STFT operation, and N_R be the number of STFT operations which is given by

$$N_R = \text{floor}\left(\frac{M-N}{N_S}+1\right). \tag{1}$$

We propose the following transformation for both noise smoothing and data size reduction:

$$\mathbf{x}_i[k] = \frac{1}{N_R}\sum_{i=1}^{N_R}|X_i[k]| \tag{2}$$

where $\mathbf{x}_i \in \mathbb{R}^N$ is a row vector representing the classification input vector for the i^{th} measurement, and

$$X_i[k] = \sum_{n=0}^{N-1}\mathbf{y}_i\left[n+(i-1)N_s\right]\exp\left(-i2\pi kn/N\right) \tag{3}$$

where $\mathbf{y}_i \in \mathbb{C}^M$ is the i^{th} original received signal from the measuring device. Please notice that the size of $\mathbf{x}_i$ is much smaller than $\mathbf{y}_i$, and $\mathbf{x}_i$ is the averaged magnitudes with lower frequency resolution. The status of the camera is kept the same during the measurement but other activities on the cell phone are varying during the measurements. Therefore, averaging in (2) reduces the variation due to non-camera activities. Likewise, decreasing the resolution helps to reduce the dimension of the input space and the size of the data.

B. Phase-II: Further Size Reduction with PCA

In order to determine the status of a camera, the first solution that comes to mind is tracking frequency components that significantly differ upon initialization of camera activity. In Fig. 1a and Fig. 1b, we provide spectrogram of two cellphones downconverted by 990 MHz when rear/front camera is on/off. These two figures are given to demonstrate the possible scenarios for diverse camera activities. The main observations from these two figures can be listed as follows:

- Some frequency components become stronger when rear/front camera is on.
- Different frequency components are activated for different cellphone vendors.
- For Alcatel phone, the same frequency components are activated for both front and rear cameras. However, front camera produces weaker signals than the rear camera.
- For ZTE phone, different signal components get stronger for rear and front cameras.

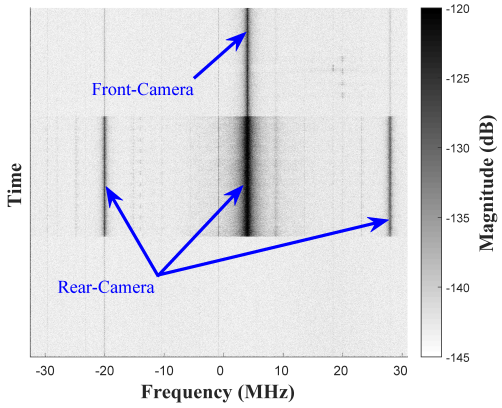

(a) Spectrogram for Alcatel phone when the camera is off, when the rear-camera is on, and when front-camera is on.

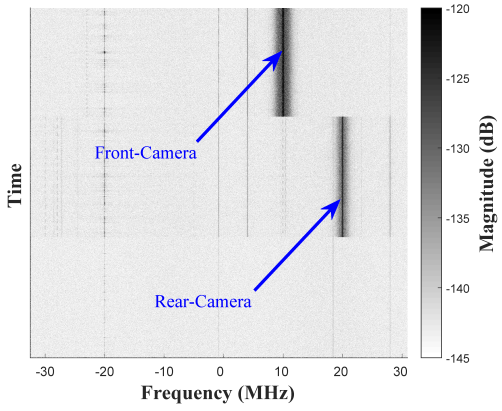

(b) Spectrogram for ZTE phone when the camera is off, when the rear-camera is on, and when front-camera is on.

Fig. 1: Spectrogram of received signals.

Because various frequency components are activated for different phones and camera status, tracking all frequency

components can cause overhead on the performance of detection algorithm. Also the frequency components and corresponding thresholds have to be set cautiously for more accurate results. To overcome these difficulties, as the second step of our method, we apply principle component analysis (PCA) which is exploited to reduce data size further while keeping the variation between classes as much as possible.

Assuming $M \gg N$, the method given in Section II-A decreases the size of data considerably. Likewise, PCA helps to decrease the data size further by keeping the important features regarding to clusters. To apply PCA, we first need to generate the data matrix $\mathbf{X}$ which is given by

$$\mathbf{X} = \begin{bmatrix} — & \hat{\mathbf{x}}_1 & — \\ — & \hat{\mathbf{x}}_2 & — \\ & \vdots & \\ — & \hat{\mathbf{x}}_m & — \end{bmatrix} \tag{4}$$

where m is the number of measurements and $\hat{\mathbf{x}}_i$ is the transformed version of $\mathbf{x}_i$ given by

$$\hat{\mathbf{x}}_i[k] = 10\log_{10}\left(|\mathbf{x}[k]|^2\right). \tag{5}$$

Here, each column of $\mathbf{X}$ represents an averaged frequency component in dB-domain.

The reason behind transforming the input space into dB-domain is as follows: DC-component magnitudes of the measurements are pretty large compared to other frequency components, therefore, dimension reduction with PCA in linear domain can result in over-weighted contribution from DC components. This might lead to the loss of the variation among higher frequency components and consequently result in inaccurate classification. Hence, applying linear to dB-domain transformation decreases the dominance of DC-components, and increases the effect of other frequency components on PCA output.

Let $\mathbf{Y} = \mathbf{X}^T\mathbf{X}$ and its eigen-decomposition be

$$\mathbf{Y} = \mathbf{\Lambda}\ \boldsymbol{V}\boldsymbol{\Lambda}^{\boldsymbol{T}} \tag{6}$$

where $(\bullet)^T$ is the Hermitian transpose of its argument. Then, the size of the collected data is decreased further by projecting $\mathbf{X}$ into a new space $\boldsymbol{\mathcal{X}} \in \mathbb{R}^{m\times K}$ as follows:

$$\boldsymbol{\mathcal{X}} = \boldsymbol{X}\mathbf{\Lambda_K}\mathbf{V_K} \tag{7}$$

where $\mathbf{\Lambda_K} \in \mathbb{R}^{N\times K}$ contains K eigenvectors corresponding to the largest K eigenvalues of $\mathbf{Y}$, and $\mathbf{V_K} \in \mathbb{R}^{K\times K}$ is a diagonal matrix whose entries are square-root of the multiplicative inverse of corresponding eigenvalues. With this step, the dimension of the feature vectors reduces to only K, which could be beneficial to implement less complex detection methods for clustering.

III. Testing Methodology to Unveil the Status of a Camera

In supervised learning, the method that is obtained in training is utilized during the testing phase to correctly classify the received signals. In that respect, in Section II, a methodology is introduced to obtain a model for classifying camera activities. The model contains three parameters: The transformed data matrix $\boldsymbol{\mathcal{X}}$, the eigenvector matrix $\mathbf{\Lambda_K}$, and the diagonal eigenvalue matrix $\mathbf{V_K}$. In order to cluster the data points by using the developed method, we propose to apply k-Nearest Neighbors (k-NN) algorithm. The overall procedure for classification can be listed as follows:

- Measure the emanated signal for T seconds assuming the status of the camera is unchanged in this time interval.
- Apply the method given in Section II-A to reduce the effect of undesired emanated signals and channel noise, and decrease the size of the collected data.
- Apply PCA to obtain the model ($\boldsymbol{\mathcal{X}}$, $\mathbf{\Lambda_K}$, $\mathbf{V_K}$) that will be exploited in testing phase.
- Collect the testing signal $\mathbf{z}$ with the measuring instrument and apply the noise and size reduction technique introduced in Section 2.
- Transform $\mathbf{z}$ into dB-domain as given in (5) to obtain $\hat{\mathbf{z}}$.
- Produce the input for k-NN algorithm by projecting the test signal into the space defined by the model as:

$$\boldsymbol{\mathcal{Z}} = \hat{\mathbf{z}}\ \mathbf{\Lambda}_{\boldsymbol{K}}\mathbf{V_K}. \tag{8}$$

- Apply k-NN algorithm to estimate the status of the camera by utilizing $\boldsymbol{\mathcal{X}}$ and $\boldsymbol{\mathcal{Z}}$.

Although k-NN algorithm is a simple tool to classify the signals, in the next section, we demonstrate that it is a practical and effective tool to accurately estimate the test signals with the given experimental setup and analysis.

IV. Experimental Results and Discussion

This section provides experimental results and discussion for identifying camera status. We demonstrate that emissions due to camera activities can leak information, and this information can be exploited for device monitoring purposes.

TABLE I: Tested phones for camera activity classification.

	Phone	Clock Frequency	Core
a)	ZTE ZFive	1.4 GHz	Quad-Core
b)	Alcatel Ideal	1.1 GHz	Quad-Core
c)	iPhoneSE	1.85 GHz	Dual-Core
d)	Samsung Centura	800 MHz	Single-Core

The setups for experiments are given in Fig. 2. We test the proposed method for various phones that are given in Table I in the same order. We also use AAronia PBS H2 near-field magnetic probe which is placed on top of the rear camera, and a signal analyzer (Keysight MXA N9020B) as the measuring device. Unless otherwise noted, the bandwidth for experiments is fixed to be 30 MHz and the signal is downconverted by 990 MHz.

A. Identifying Camera Status for a Specific Phone with Near-Field Measurements

The first experiment set is designed to illustrate whether differentiating the camera status is possible for a given phone. We consider the measurement time, T, as 5 ms, the STFT window

Fig. 2: Experimental setup for near-field measurements with phones from various vendors.

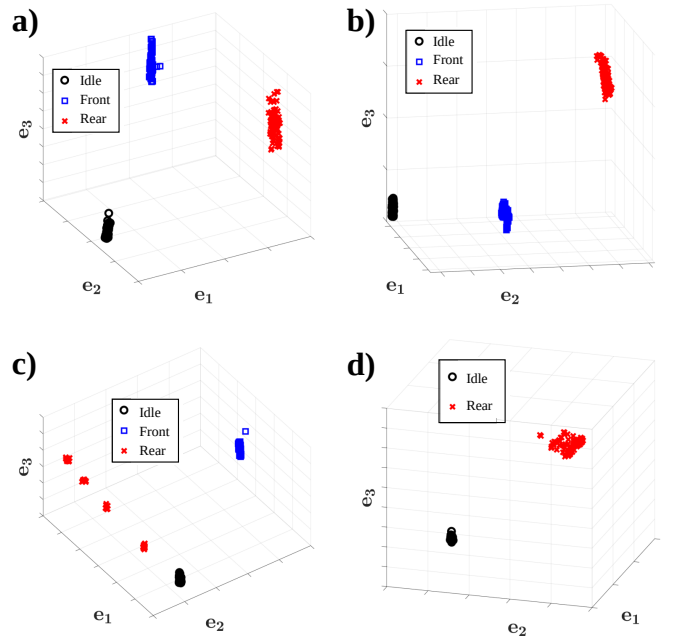

Fig. 3: Clusters obtained during training phase for near-field measurements with phones in Fig. 2, respectively.

length, N, as 4096, sampling time, T_s, as 1.3×10^{-8} (This value is device-specific), and the number of non-overlapping samples, N_S, as 7680 (This number corresponds to 0.1 ms).

Fig. 3 demonstrates the training models in the same order as in Table I when the dimension of the data, K, is reduced to 3. We need to note that the original length of the data is 384000 (This value corresponds to 5 ms of the received signal). In these models, $\mathbf{e_i}$ represents the eigenvector direction corresponding to i^{th} largest eigenvalue. We take 100 measurements for each possible scenarios. The main outcome here is that for all phones, the clusters are dense and the separation between different clusters are very clear. Another interesting observation is that the behavior of iPhoneSE is different when rear-camera is on: It also consists of some sub-clusters that are not encountered for other phones. However, all of these sub-clusters are explicitly classified and the variations within each sub-cluster at any direction is pretty small. We also need to note that Samsung phone has only rear camera, and that is why the corresponding figure has only two clusters.

For the testing part, we again perform 100 measurements for each combination of phones and camera activities, and apply the proposed method to estimate the class of each measurement. For k-NN algorithm, we check 10 nearest neighbors. The accuracy of the method with the given setup is **100%** for each model with **zero** false positive. Therefore, for a given phone, we can successfully determine whether rear/front camera is on. Also, the method presented here is a zero-overhead monitoring because no adjustment has been done to hardware or software of the devices.

B. Identifying Camera Status and Model with Near-Field Measurements when Rear/Front Camera is On

Observing the explicit separation of clusters for each phone, we question the possibility of estimating the phone model based on the signal emanated when rear/front camera is on. In other words, the training matrix contains measurements captured when rear or front camera is on for the cellphones given in Table I. We do not include the data corresponding to camera-is-off case for training because there are small differences between signals among different vendors that are not effective enough to be distinguished by the proposed method. As much as we cannot determine the model of the phone when the camera is inactive, it is still possible to determine that the camera is inactive. In short, if there is a camera activity from the phones listed in Table I, we can successfully determine from which phone and camera (rear or front) the emanated signal comes from. Also, if there are no active cameras, we can conclude that with zero false positives.

We follow the same procedure in Section II to generate the model parameters. Again, we collect 100 signals for each experimental setup. The model of data after noise and dimension reduction is given in Fig. 4. In this figure, we provide clusters for each phone when rear/front camera is on except Samsung phone because it has only one rear camera. We observe that the clusters are well separated, and the distance between cluster centroids is larger than any in-group variation at any direction.

The next step is to collect test signals, and apply noise and size reduction methods proposed in Section II. In that respect, we capture 100 test signals for each class, and follow exactly the same procedure given in Section III. Although

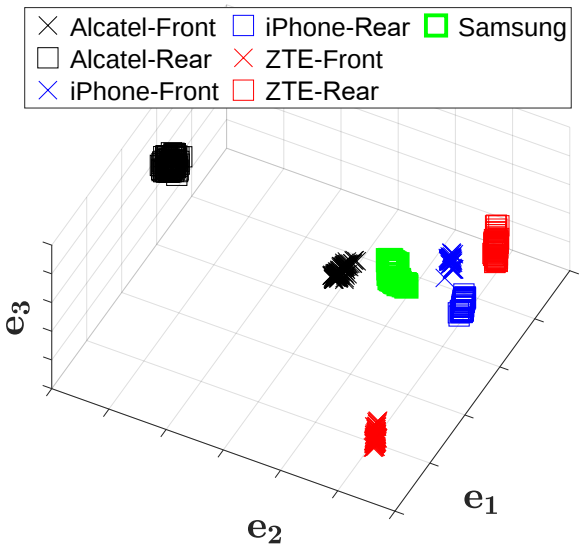

Fig. 4: Clusters obtained during training phase for near-field measurements when rear/front camera is on.

some clusters look very close to each other, we obtain **100%** accuracy and **zero** false negative for each group.

C. Identifying Camera Status with Far-Field Measurements

Near-field measurements provide notably promising results to identify camera status and phone model. Further to that, it is even more significant and practical to determine the camera activity from far-field measurements for zero-overhead monitoring.

The setup for far-field measurements is given in Fig. 5. We use a lab-made planar antenna that is designed in our lab and operates around 1 GHz [24]. The measurements are done at a distance of 5 meters. We apply the same procedure to generate the classification model as introduced in Section II. We observe that the variations within clusters are larger compared to the near-field measurements. Also, the distance between cluster centroids is smaller as given in Fig. 6a, therefore, we expect to have inaccurate estimations. Especially, when the same frequency components are active for both rear and front cameras, it is very tricky to determine whether the active camera is the rear or front one. An example of such a situation is given in Fig. 6b for experiments done with Alcatel phone. As it can be noted in Fig. 6b, the same frequency components are dominant during both rear and front camera activities, with very slight amplitude differences, which makes distinguishing those two classes very challenging.

Another critical observation is that the emanated signal is extremely weak even for near-field measurements when rear camera of iPhone is on. This extremely weak signal is further attenuated due to the distance for far field measurements and consequently it is almost impossible to capture the signal from 5 m distance. Therefore, we update our goal for iPhone as distinguishing the status of the front camera.

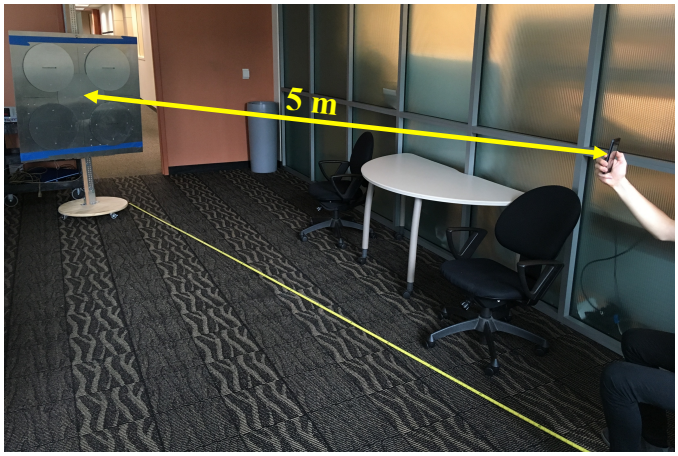

Fig. 5: Experimental setup for far-field measurements.

TABLE II: Testing misclassification for each phone.

	ZTE	**Alcatel**	**iPhoneSE**	**Samsung**
Error	0%	1.5%	0%	3%

The misclassification rates for each phone are given in Table II. We observe that the error probabilities are less than 3%, which supports our initial hypothesis that accurate estimation of camera status is possible even from some distance.

Lastly, we investigate the effect of phone rotation on the received signal power. In that respect, we perform experiments with the setup given in Fig. 5 from a distance of 50 cm. We assume the zero degree position corresponds to the position when the phone is parallel to the ground and heads to the right hand side of the figure. We observe that the power loss shows dependency on the rotation of phone such that the loss is minimum when the phone heads up, and maximum when it is horizontal. Although there are small power variations in received signal power, we could conclude that emanated signal is relatively rotation-invariant.

V. Conclusions

We investigate unintended radiated emissions to identify whether rear/front camera is on/off for various cellphone models. Both far-field and near-field measurements are analyzed to estimate the status of a camera. A supervised learning methodology is applied to achieve better accuracy results. In the training phase, we collect data for possible combinations of phone models and camera activities followed by two-phase-dimension-reduction method for better and effective classification. The first dimension-reduction phase averages magnitudes of frequency components of a sliding window. Then, we apply PCA technique to reduce the dimension further, and build a model for the training data. In the testing phase, k-Nearest-Neighbors (k-NN) algorithm is utilized to group each test signal based on the model. Finally, we provide some experimental results. We achieve a perfect accuracy rate with no false positive in near-field measurements. Also, we demonstrate that the status of camera can be detected at a

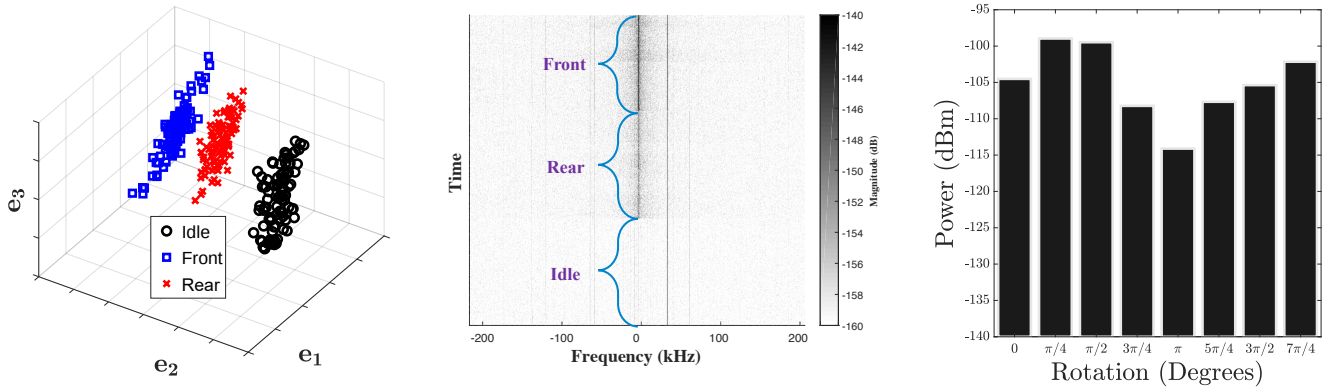

(a) Clusters of Alcatel for the far-field measurements.

(b) Spectrogram of Alcatel phone for distance measurements.

(c) The received power for different phone rotations.

Fig. 6: Experimental results for far-field measurements.

distance of 5 m, which illustrates the severity of information leakages due to camera activities.

REFERENCES

[1] P. Kocher, "Timing attacks on implementations of Diffie-Hellman, RSA, DSS, and other systems," in *Proceedings of CRYPTO'96, Springer, Lecture notes in computer science*, 1996, pp. 104–113.

[2] B. W. Lampson, "A note on the confinement problem," *Commun. ACM*, vol. 16, no. 10, pp. 613–615, Oct. 1973. [Online]. Available: http://doi.acm.org/10.1145/362375.362389

[3] W. Schindler, "A timing attack against RSA with Chinese remainder theorem," in *Proceedings of Cryptographic Hardware and Embedded Systems - CHES 2000*, 2000, pp. 109–124.

[4] D. Boneh and D. Brumley, "Remote Timing Attacks are Practical," in *Proceedings of the USENIX Security Symposium*, 2003.

[5] J. Brouchier, T. Kean, C. Marsh, and D. Naccache, "Temperature attacks," *Security Privacy, IEEE*, vol. 7, no. 2, pp. 79–82, March 2009.

[6] P. Kocher, J. Jaffe, and B. Jun, "Differential power analysis: leaking secrets," in *Proceedings of CRYPTO'99, Springer, Lecture notes in computer science*, 1999, pp. 388–397.

[7] T. S. Messerges, E. A. Dabbish, and R. H. Sloan, "Power analysis attacks of modular exponentiation in smart cards," in *Proceedings of Cryptographic Hardware and Embedded Systems - CHES 1999*, 1999, pp. 144–157.

[8] L. Goubin and J. Patarin, "DES and Differential power analysis (the "duplication" method)," in *Proceedings of Cryptographic Hardware and Embedded Systems - CHES 1999*, 1999, pp. 158–172.

[9] S. Chari, C. S. Jutla, J. R. Rao, and P. Rohatgi, "Towards sound countermeasures to counteract power-analysis attacks," in *Proceedings of CRYPTO'99, Springer, Lecture Notes in computer science*, 1999, pp. 398–412.

[10] M. Backes, M. Dürmuth, S. Gerling, M. Pinkal, and C. Sporleder, "Acoustic side-channel attacks on printers," in *19th USENIX Security Symposium, Washington, DC, USA, August 11-13, 2010, Proceedings*, 2010, pp. 307–322.

[11] Y. Tsunoo, T. Saito, T. Suzaki, M. Shigeri, and H. Miyauchi, "Cryptanalysis of des implemented on computers with cache," in *International Workshop on Cryptographic Hardware and Embedded Systems*. Springer, 2003, pp. 62–76.

[12] D. Gullasch, E. Bangerter, and S. Krenn, "Cache games–bringing access-based cache attacks on aes to practice," in *Security and Privacy (SP), 2011 IEEE Symposium on*. IEEE, 2011, pp. 490–505.

[13] A. Zajic and M. Prvulovic, "Experimental demonstration of electromagnetic information leakage from modern processor-memory systems," in *IEEE Transactions on Electromagnetic Compatibility, Volume: 56, Issue: 4,*, 2014, p. 885893.

[14] D. Agrawal, B. Archambeult, J. R. Rao, and P. Rohatgi, "The EM side-channel(s)," in *Proceedings of Cryptographic Hardware and Embedded Systems - CHES 2002*, 2002, pp. 29–45.

[15] D. Genkin, I. Pipman, and E. Tromer, "Get your hands off my laptop: Physical side-channel key-extraction attacks on pcs," in *Cryptographic Hardware and Embedded Systems CHES 2014*, ser. Lecture Notes in Computer Science, L. Batina and M. Robshaw, Eds. Springer Berlin Heidelberg, 2014, vol. 8731, pp. 242–260. [Online]. Available: http://dx.doi.org/10.1007/978-3-662-44709-3_14

[16] B. Yilmaz, A. Zajic, and M. Prvulovic, "Modelling jitter in wireless channel created by processor-memory activity," in *IEEE International Conference on Acoustics, Speech and Signal Processing, ICASSP 2018*, 04 2018, pp. 2037–2041.

[17] B. B. Yilmaz, R. Callan, M. Prvulovic, and A. Zajić, "Quantifying information leakage in a processor caused by the execution of instructions," in *Military Communications Conference (MILCOM), MILCOM 2017-2017 IEEE*. IEEE, 2017, pp. 255–260.

[18] B. B. Yilmaz, R. Callan, A. Zajic, and M. Prvulovic, "Capacity of the em covert/side-channel created by the execution of instructions in a processor," *IEEE Transactions on Information Forensics and Security*, vol. 13, no. 3, pp. 605–620, 2018.

[19] W. Van Eck, "Electromagnetic radiation from video display units: an eavesdropping risk?" *Computers & Security*, vol. 4, no. 4, pp. 269–286, 1985.

[20] M. G. Kuhn, "Compromising emanations: eavesdropping risks of computer displays," Ph.D. dissertation, University of Cambridge, 2002.

[21] M. Alam, H. A. Khan, M. Dey, N. Sinha, R. L. Callan, A. G. Zajic, and M. Prvulovic, "One&done: A single-decryption em-based attack on openssl's constant-time blinded RSA," in *27th USENIX Security Symposium, USENIX Security 2018, Baltimore, MD, USA, August 15-17, 2018.*, 2018, pp. 585–602.

[22] A. V. Oppenheim, *Discrete-time signal processing*. Pearson Education India, 1999.

[23] F. Werner, D. A. Chu, A. R. Djordjević, D. I. Olćan, M. Prvulovic, and A. Zajić, "A method for efficient localization of magnetic field sources excited by execution of instructions in a processor," *IEEE Transactions on Electromagnetic Compatibility*, vol. 60, no. 3, pp. 613–622, 2018.

[24] P. Juyal, S. Adibelli, N. Sehatbakhsh, and A. Zajic, "A directive antenna based on conducting disks for detecting unintentional em emissions at large distances," *IEEE Transactions on Antennas and Propagation*, vol. 66, no. 12, pp. 6751–6761, 2018.